Rare earth borocarbides: Electronic structure calculations and electric field gradients

M. Diviš
Department of Electron Systems, Charles University, Ke Karlovu 5, 121 16 Praha 2, Czech Republic

K. Schwarz and P. Blaha
Institut für Physikalische und Theoretische Chemie, Technische Universität Wien, Getreidemarkt 9, A-1060 Wien, Austria

G. Hilscher and H. Michor
Institut für Experimentalphysik, Technische Universität Wien, Wiedner Hauptstrasse 8–10, A-1040 Wien, Austria

S. Khmelevskyi
Department of Electron Systems, Charles University, Ke Karlovu 5, 121 16 Praha 2, Czech Republic
(Received 23 March 2000)

The electronic structure of $R\mathrm{Ni_2B_2C}$ (R=Y, La, Pr–Tm, Lu) is systematically studied using density functional theory (DFT). The partially occupied $4f$ states are assumed to be localized for both the light and heavy rare earths (R=Pr, Nd, Sm, Tb, Dy, Ho, Er, Tm) and treated in the ''open core approximation.'' In the case of Gd (Lu) the $4f$ states are treated both as itinerant and as part of the atomiclike core states. The calculations of the electronic density of states (DOS) show that the Fermi energy E_f is located in a pronounced peak for R=Y, Dy, Ho, Er, Tm, and Lu. This peak starts to be broadened for R=Tb, Gd, and Sm and finally disappears for R=Pr, Nd. This reduction is large enough to explain the depression of superconductivity to below 3 K in the light rare-earth borocarbides. Additional calculations of the Hopfield parameters support this conclusion. The charge density distribution and general features of the bonding mechanism are discussed. The relations between the DOS in the vicinity of E_f and the lattice parameters a,c and the free internal structural parameter z_B of boron are studied using the DFT total energy and force calculations. The total energy is very sensitive to the c/a ratio and the optimum DFT values of c/a and z_B are close to those observed in the experiment. The electric field gradients (EFG) on the Gd- ($\mathrm{GdNi_2B_2C}$) and B-site ($\mathrm{YNi_2B_2C}$) are calculated and agree with experimental data. We also point out that the physical origin of this relatively large EFG on the Gd site results from a strong cancellation between positive $6p$-$6p$ and negative $5p$-$5p$ contributions.

I. INTRODUCTION

The new class of rare-earth transition-metal borocarbides with the general formula $R\mathrm{Ni_2B_2C}$ attracted the interest of many groups, because of their wide variety of physical properties: Compounds with R=Y and Lu exhibit fairly high superconducting transition temperatures T_c of about 15–16 K;[1–3] magnetism coexists with superconductivity for R=Dy, Ho, Er, and Tm[4] whereas only antiferromagnetic order occurs for R=Pr, Nd, Sm, Gd, and Tb (see, e.g., Ref. 5). The Néel temperatures T_N are of the same order of magnitude as T_c and scale for both the light- and heavy-rare-earth borocarbides approximately with the de Gennes factor $(g_J-1)^2J(J+1)$, which is to a first approximation also the case for the depression of superconductivity for the magnetic heavy-rare-earth borocarbide superconductors. Furthermore, $\mathrm{CeNi_2B_2C}$ is a mixed valent compound[6,7] and $\mathrm{YbNi_2B_2C}$ shows heavy fermion behavior.[8,9] For a review on superconductivity and magnetism in quaternary borocarbides and boronitrides see, e.g., Ref. 10.

The electronic structure of the $R\mathrm{Ni_2B_2C}$ compounds was investigated by band structure calculations based on the density-functional theory (DFT) for R=Y,[11–15] La,[16] Gd,[17] and Lu.[14,18] Despite the layered crystal structure, which is a filled version of the $\mathrm{ThCr_2Si_2}$-type structure stabilized by the incorporation of carbon, the results of these calculations[12–14,17,18] show that the electronic structure is almost three dimensional. All elements contribute to the metallic character leading to a complex Fermi surface due to the dual band characteristics at the Fermi energy. There is good evidence from various experiments such as specific heat,[19,20] NMR,[21] and inelastic neutron scattering[22,23] (INS) that these borocarbides are conventional electron-phonon mediated superconductors with an order parameter with s-wave symmetry.[10]

The depression of T_c in the pseudoquaternary systems $\mathrm{Y_{1-x}}R_x\mathrm{Ni_2B_2C}$ and $\mathrm{Lu_{1-x}}R_x\mathrm{Ni_2B_2C}$ (where R is a heavy rare earth) follows in the dilute limit the Abrikosov Gor'kov pair-breaking relation but significant deviations are observed for the concentrated regime that result in remarkable deviations or even a breakdown of the de Gennes scaling for T_c in particular for systems $R_{1-x}R'_x\mathrm{Ni_2B_2C}$ where $T_N > T_c$ (see Refs. 24–26). Nevertheless, in view of the approximate de Gennes scaling of T_c for the magnetic heavy-rare-earth superconductors, one expects that superconductivity should occur also in the light-rare-earth borocarbides as long as electronic changes are not taken into account for the disruption of superconductivity. Mattheiss *et al.*[16] pointed out that the variation of the B-Ni-B angle has a detrimental impact upon $N(E_f)$, which explains the disappearance of superconductivity in $\mathrm{LaNi_2B_2C}$. On the other hand, x-ray absorption spectroscopy results across the whole series reported by Pellegrin

et al.[27] revealed no significant variation in the unoccupied density of states (DOS) close to the Fermi energy. This is in contrast to the suggestion that the loss of superconductivity for the light-rare-earth compounds is due to a reduction of $N(E_f)$. However, specific-heat results[19] are in agreement with the calculated reduced $N(E_f)$ for $LaNi_2B_2C$. Unfortunately, direct experimental evidence for the reduction of $N(E_f)$ via the determination of the electronic specific heat in the magnetic rare-earth compounds is prevented by the large magnetic background. Hence, a systematic band-structure study across the rare-earth borocarbide series is presented in this paper in order to clarify why the light-rare-earth borocarbides are nonsuperconducting.

The electronic structure of the RNi_2B_2C compounds with either an unoccupied (Y, La), half-occupied (Gd), or fully occupied $4f$ shell (Lu) was studied intensively, whereas the compounds with a partially occupied $4f$ shell were investigated much less.[10] The discrete variational embedded-cluster approach was used to investigate the electronic structure of $R=$Pr, Nd, Sm, Gd, Ho, and Tm compounds.[28] This work was based on a nonrelativistic spin-polarized approximation and did not include the very interesting cases of $R=$Tb and Dy, the former compound being nonsuperconducting and latter being a superconductor with $T_N > T_c$. Here we performed electronic structure calculations for $R=$Y, La, Pr, Nd, Sm, Gd, Tb, Dy, Ho, Er, Tm, and Lu compounds using the full-potential linearized augmented plane-wave method,[32] which is well suited because of its wide applicability and high accuracy. The self-consistent calculations allow us to study in detail the DOS for $R=$Pr–Tm compounds and to find arguments for the absence of a superconducting transition in the case of $R=$Pr, Nd, Sm, Gd, and Tb compounds.

This paper is organized as follows. The details of the crystal structure, the electronic structure calculations, and the methods used to treat the localized $4f$ states are described in Sec. II A, II B, and II C, respectively. Section II D presents the details of EFG calculations and the necessary modifications to treat the $4f$ electron systems. In Secs. III A, III B, and III C we provide results and discussions of the electronic structure, valence charge densities, and EFG of rare-earth borocarbides, respectively. The important conclusions from our DFT calculations are given in the last section.

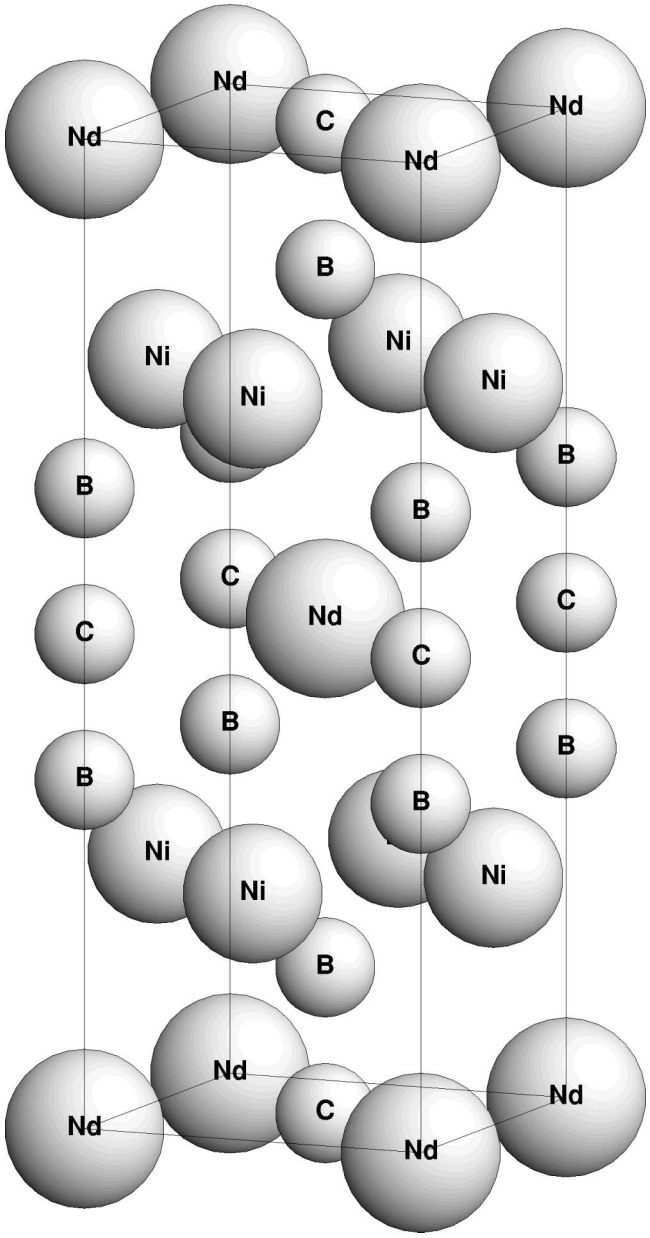

FIG. 1. The crystal structure of $NdNi_2B_2C$.

II. COMPUTATIONAL ASPECTS

A. Structure

All compounds under investigation crystallize in the body centered tetragonal structure (space group I4/*mmm*). The structure consists of *R*-C planes separated by Ni-B layers stacked along the *c* axis (see Fig. 1). The crystal data (with the exception of $R=$La, Sm, Gd, and Lu) were taken from Lynn *et al.*,[5], who determined the lattice parameters *a*, *c*, and the structural parameter z_B (for the boron $4e$ position), using neutron diffraction. In the case of $LaNi_2B_2C$, $SmNi_2B_2C$, $GdNi_2B_2C$, and $LuNi_2B_2C$, we used the structural data of Siegrist *et al.*[31]

B. Electronic structure calculations

The calculations presented here are based on (DFT), using the local spin-density approximation (LSDA) or the generalized gradient approximation (GGA) in the recent parameterization of Perdew-Burke-Ernzerhof.[29] For our calculations, we use the linearized augmented plane wave (LAPW) method, in which the unit cell is partitioned into spheres (with a muffin-tin radius R_{MT}) centered at the atomic positions and an interstitial region. In the latter, the Bloch wave functions are expanded using plane waves that are augmented by atomiclike functions (numerical radial functions multiplied by spherical harmonics) inside the spheres. The effective one-electron DFT potential as well as charge density are treated without any shape approximation (i.e., termed full-potential scheme). A good summary of LAPW can be found in the book by Singh.[30]

In the present study, the full-potential LAPW package, WIEN97,[32] was used. In general, we treated the valence states scalar relativistically, but in some calculations (for $GdNi_2B_2C$ and $TbNi_2B_2C$) we included the spin-orbit coupling in a second-order variational step, as originally sug-

gested by Koelling and Harmon.[33] The LAPW sphere radii are $R_{MT}=2.8$, 2.3, 1.35, and 1.35 a.u. for *R*, Ni, B, and C, respectively, but in YNi_2B_2C the sphere radii had to be reduced to 2.7, 2.25, 1.35, and 1.28 a.u. for Y, Ni, B, and C, respectively. Inside the atomic spheres, the Y $5s$, $5p$, $4d$; *R* $6s$, $6p$, $5d$; Lu $6s$, $6p$, $5d$, $4f$; Ni $4s$, $4p$, $3d$; B $2s$, $2p$; and C $2s$, $2p$ are described by numerical solutions $u_l(\epsilon_l,r)$ of the radial Schrödinger equation and the corresponding energy derivatives $\partial u_l/\partial\epsilon$ while in the interstitial region plane-wave functions were used. The energies ϵ_l were suitably chosen in order to describe the occupied valence states. In order to provide an accurate treatment of the high-lying extended core states (''semicore states'') with a principal quantum number of one less than the valence states (Y $4s$, $4p$; *R* $5s$, $5p$; Ni $3p$; C $2s$) the standard LAPW basis set is extended with local orbitals.[30] The core states were treated relativistically including spin-orbit coupling and the corresponding core charge densities are obtained self-consistently. A well-converged basis of approximately 950 plane-wave basis functions plus additional *s* and *p* local orbitals was used. During the iterations to self-consistency, the Brillouin zone was sampled using 102 special *k* points in the irreducible wedge of the zone. These details of our calculations are similar to Refs. 11 and 18, which provided highly accurate results for $LuNi_2B_2C$ and YNi_2B_2C.

C. Treatment of the 4*f* states

In the current literature there is still a controversy about the treatment of the electronic $4f$ states. This can be illustrated, for example, in the case of bulk ferromagnetic Gd. Models, which treat the $4f$ states as either itinerant electrons, or completely localized core-like states, or use nonspin polarized DFT potentials, can be definitely excluded, since Gd is a strong ferromagnet with a magnetization of about $7\mu_B$/atom and a Curie temperature of 289 K. In some calculations the $4f$ states were treated as itinerant band states but spin polarized (see, e.g., Refs. 34–37). Such self-consistent calculations, which are usually based on LSDA, yield a DOS at the Fermi level, $N(E_f)$, spanning a wide range (of about 25 to 47 states/Ry, see Ref. 37), but larger than the experimental value of 21 states/Ry reported by Wells *et al.*[38] This is quite unusual, since normally the electron-phonon coupling and additional electronic correlations lead to an enhancement of $N(E_f)$ above the bare LSDA value. Therefore, another approach has been advocated for Gd, namely, that one should treat the $4f$ states as localized core electrons in LSDA.[39–41] It is worth noting that there has been some controversy in the literature whether or not this is a good approximation.[42] Such intensive discussions about the treatment of the $4f$ states in pure Gd metal motivated us to undertake a careful theoretical study concerning this issue for the rare-earth borocarbides and the $GdNi_2B_2C$ compound in particular.

In order to simulate localized $4f$ states we switch off the hybridization between $4f$ and valence states and treat the *R* $4f$ states in the spherical part of the potential as atomiclike core states (open-core treatment). The relevant cases are characterized by the integer occupation number $N=2$, 3, 5, 7, 8, 9, 10, 11, and 12 for $R=$Pr, Nd, Sm, Gd, Tb, Dy, Ho, Er, and Tm, respectively. The same approach was successfully used in our earlier investigation in $PrBa_2Cu_2O_7$.[43] A comprehensive discussion of the ''open-core treatment'' can be found in Ref. 44. Since we are mainly interested in the behavior of the normal paramagnetic state above T_c and T_N, we performed nonspin-polarized studies using local-density approximation (LDA) for a reference ground state which is not magnetically ordered. This approach is model *A* and quoted in the following as $R(A)$.

To test the limits of these results, we also performed spin-polarized calculations for $R=$Gd, in which we treated the $4f$ states as follows: Gd(B) $4f$ electrons as band states, ferromagnetic LSDA calculation; Gd(C) $4f$ electrons as band states, ferromagnetic GGA calculation; Gd(D) $4f$ electrons as core states, ferromagnetic LSDA calculation; Gd(E) $4f$ electrons as band states, ferromagnetic GGA calculation including spin-orbit interaction.

In the case of $R=$Tb the $4f$ electrons should be treated as core states, because otherwise the $4f$ states are situated at the Fermi level producing a very high and unphysical density of states at E_f. Therefore, the $4f$ states were treated as follows: Tb(B) $4f$ electrons as core states, ferromagnetic LSDA calculations; Tb(C) $4f$ electrons as core states, nonmagnetic GGA calculations; Tb(D) $4f$ electrons as core states, nonmagnetic LDA calculations including spin-orbit interaction.

In the case of $R=$Lu the $4f$ valence states are fully occupied. In our calculations the corresponding *f* bands were found to lie 4.9 eV below E_f and hybridization with the remaining valence states is very small in agreement with Ref. 18. Thus almost no difference in our results concerning the DOS around E_f were found assuming the ''normal'' valence $4f$ states or ''open core'' $4f$ states. In the case of $R=$Ce($N=1$) and Yb ($N=13$) the $4f$ states are very close to E_f and moreover the hybridization between the $4f$ states and valence states definitely cannot be neglected. As mentioned above $CeNi_2B_2C$ and $YbNi_2B_2C$ are considered to be an intermediate valence[6,7] and heavy fermion[8,9] compound, respectively. Thus, the theoretical study of the electronic structure of these latter two compounds is beyond the scope of this paper.

D. Electric field gradient

The largest effect of pair breaking due to the rare-earth spin moments is expected for $GdNi_2B_2C$. Therefore, the hyperfine field and the electric field gradient (EFG) at the Gd site were investigated by means of ^{155}Gd Mössbauer spectroscopy.[45] The EFG can also be obtained theoretically from the total charge density. Blaha *et al.*[46] used for the first time the LAPW method for the calculation of EFG in solids. During the last decade, this method was used to investigate many substances and its feasibility for complex structures was demonstrated, e.g., by successful calculations for high-T_c superconductors.[47] It was found that the EFG provides a very sensitive probe of the anisotropy of the charge densities. It can be expected to be a particularly good probe of the occupations of the different *R* *p*, *d*, and *f* orbitals in the $GdNi_2B_2C$ system since the spherically symmetric component of the charge density does not contribute to the EFG and the largest contribution comes from the interior of the ion. As the calculated EFG can be very sensitive to small changes in the charge distribution, especially near the nucleus, highly

accurate calculations are needed. In the present work we focus on the Gd site and study the influence of different methods of treating localized and highly correlated $4f$ states on the calculated value of the EFG. We were also interested in a comparison of our results with the earlier calculations of Coehoorn,[17] who used the augmented spherical wave (ASW) method but employed the atomic-spheres approximation (ASA), in which the crystal potential within the sphere around each atom is treated as spherically symmetric.

The electric-field gradient is defined as the second derivative of the Coulomb potential at the nucleus, written as a traceless tensor. It can be computed directly from the charge density using a method developed by Schwarz *et al.*,[47] which was successfully applied to various systems. This method is based on the full potential LAPW representation of the charge density:

$$\rho(\vec{r}) = \sum_{LM} \rho_{LM}(r) Y_{LM}(\hat{r}), \tag{1}$$

inside sphere and

$$\rho(\vec{r}) = \sum_{\vec{K}} \rho_{\vec{K}} e^{i\vec{K}\cdot\vec{r}}, \tag{2}$$

in the interstitial space, where $Y_{LM}(\hat{r})$ means symmetrized spherical harmonics (lattice harmonics). The charge density coefficients $\rho_{LM}(r)$ can be obtained from the LAPW basis wave functions

$$\rho_{LM} = \sum_{E_{n\mathbf{k}} < E_F} \sum_{l,m} \sum_{l',m'} R_{lm}(r) R_{l'm'}(r) G_{Lll'}^{Mmm'}, \tag{3}$$

where $G_{Lll'}^{Mmm'}$ are the Gaunt numbers and $R_{lm}(r) = A_{lm} u_l(r) + B_{lm} \dot{u}_l(r)$ denote the LAPW radial wave functions of state $E_{n\mathbf{k}}$ in the standard notation.[47] For the EFG calculation only the $L=2$ terms near the nucleus are needed. In the case of tetragonal site symmetry the anisotropy parameter of the EFG tensor $\eta = 0$ and the EFG can be written as

$$V_{zz} = \sqrt{\frac{5}{4\pi}} 2 V_{20}(0). \tag{4}$$

In the limit $r \to 0$ the asymptotic form of the potential yields

$$V_{20}(0) = -C_{20} \int_0^R \frac{\rho_{20}(r)}{r} dr + C_{20} \int_0^R \rho_{20}(r) \left(\frac{r}{R}\right)^5 r^{-1} dr + \frac{5 C_{20}}{R^2} \sum_{\vec{K}} V(\vec{K}) j_2(KR) Y_{20}(\hat{K}), \tag{5}$$

with $C_{20} = 2\sqrt{4\pi/5}$ and the spherical Bessel function j_2. The first term is called valence EFG and originates from the asphericity of the valence charge density inside the atomic sphere ($R = R_{MT}$). The second and third terms (called lattice EFG) arise from the boundary value problem and from charge contributions outside the considered sphere, respectively. For each spin direction the nonspherical charge density can be resolved into l-l' contributions, which come from the product of the LAPW radial wave functions within the atomic sphere with angular momentum l and l', respectively. The usual procedure is to calculate only contributions up to $l = l' = 2$.[48] In the case of $GdNi_2B_2C$ the LSDA (GGA) calculations with itinerant $4f$ states [models Gd(B), Gd(C), and Gd(E)] give a significant Q_f charge inside the Gd sphere (see Table III). Therefore, the contributions from partial f orbitals ($l = l' = 3$; $-3 \leq m \leq 3$) will be quite large and the resulting f-f contribution originates from strong cancellations of these five m contributions (f electrons in states $m = \pm 2$ do not contribute to the EFG). For those reasons we have tested possible contributions from orbitals $l \leq 5$, $l' \leq 5$.

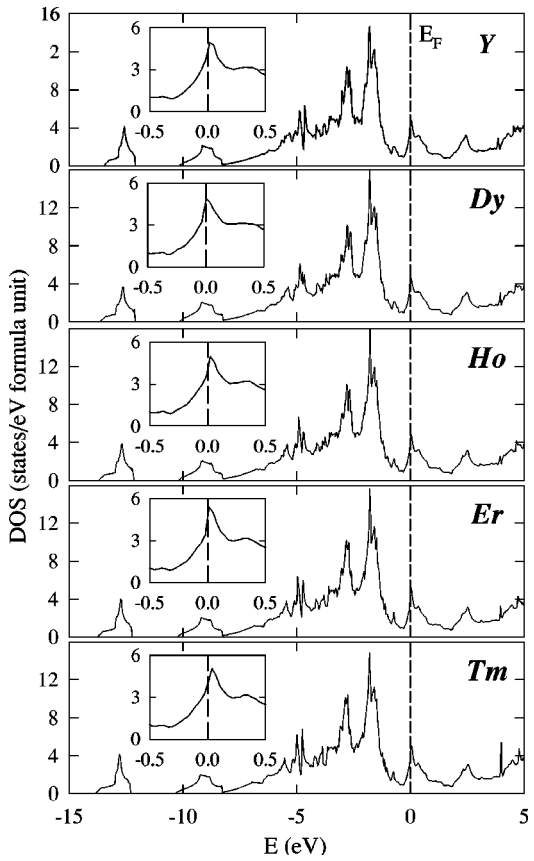

FIG. 2. Total DOS of RNi_2B_2C (R=Y, Dy, Ho, Er, and Tm). The insets show the details of DOS around the Fermi energy.

III. RESULTS AND DISCUSSION

A. Electronic properties

The total DOS are shown for the superconducting RNi_2B_2C ($R=Y$, Dy, Ho, Er, Tm) compounds in Fig. 2. The most noteworthy aspect is the occurrence of a sharp peak close to the Fermi energy E_f, which originates mainly from of Ni $3d$ states but also involves contributions from all other atoms and the interstitial region (see Table I). Our results for YNi_2B_2C are in perfect agreement with those of Singh.[11] This peak in the DOS involves Ni $3d$ states that are split from the main Ni $3d$ complex by more than 1 eV. The values of $N(E_f)$ for those RNi_2B_2C compounds are ranging from 4.3 (Y) to 4.02 states/eV (Tm), which corresponds to a linear electronic specific heat coefficient γ ranging from 10.0 to 9.4 mJ/mol K^2. For the nonsuperconducting borocarbides R =Pr, Nd, Sm, Gd, and Tb the resulting DOS curves are shown in Fig. 3. The Tb system exhibits still the relevant peak but its amplitude is already reduced. Going from Tb to

TABLE I. Data for $R\mathrm{Ni_2B_2C}$ with R=Y, Dy, Ho, Er, Tm, Lu: Site projected partial charges Q_i (in electrons) of the valence states inside R and Ni atomic spheres; the total DOS $N(E_F)$ (in states/eV f.u.), as well as its decomposition into site projected and interstitial region $N_I(E_F)$ contributions.

C	Y	Dy	Ho	Er	Tm	Lu
$Q_s(R)$	2.147	2.179	2.192	2.205	2.218	2.243
$Q_p(R)$	6.038	6.095	6.122	6.147	6.171	6.213
$Q_d(R)$	0.906	1.018	1.018	1.017	1.020	1.005
$Q_f(R)$	0.061	0.079	0.079	0.080	0.083	0.086
Q_s(Ni)	0.437	0.469	0.470	0.471	0.475	0.473
Q_p(Ni)	6.458	6.504	6.509	6.514	6.523	6.524
Q_d(Ni)	8.247	8.312	8.310	8.310	8.312	8.308
Q_f(Ni)	0.022	0.026	0.027	0.027	0.028	0.028
$N(E_F)$	4.31	4.16	4.04	4.32	4.02	4.06
$N_R(E_F)$	0.41	0.39	0.38	0.38	0.41	0.40
$N_Ni(E_F)$	2.20	2.48	2.16	2.64	2.31	2.30
$N_B(E_F)$	0.28	0.20	0.20	0.21	0.23	0.25
$N_C(E_F)$	0.11	0.10	0.11	0.12	0.13	0.15
$N_I(E_F)$	1.31	0.99	1.19	0.76	0.94	0.96

Gd the peak is washed out even more but still a maximum is present around E_f. Finally for Sm, Nd, and Pr the DOS peak is almost completely removed and a small valley with a width of about 0.5 eV appears. In the case of Pr and Nd the Fermi level is situated in a minimum of the DOS (see insets of Fig. 3).

Mattheiss *et al.*[16] suggested from his DFT calculations for the La and Lu compounds that the reduced DOS at E_f of La

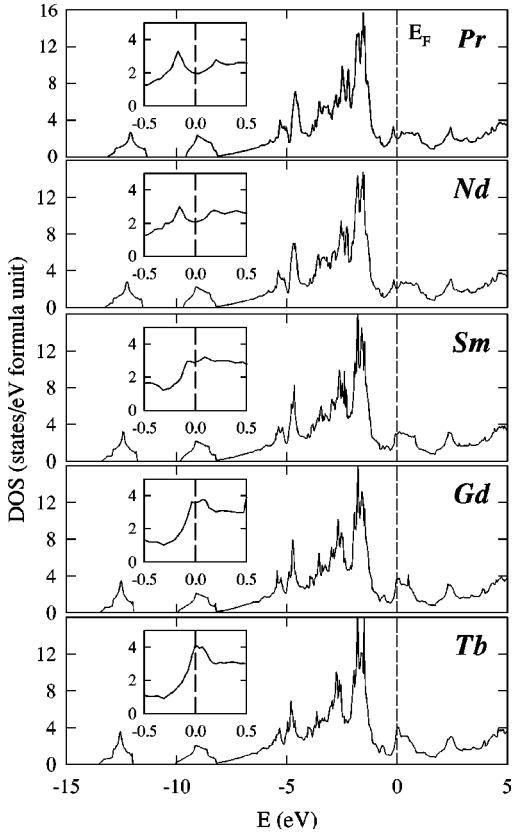

FIG. 3. Total DOS of $R\mathrm{Ni_2B_2C}$ (R=Pr, Nd, Sm, Gd, and Tb). The insets show the details of DOS around the Fermi energy.

is associated with the change in the tetrahedral NiB_4 coordination geometry. The main structural changes going from R=La to Lu involve an increase of the B-Ni-B tetrahedral angle (from 102° to 108°).[16] This is also confirmed by a detailed structural analysis by Lynn *et al.*[5] who discuss the atomic displacements when replacing Pr by Tm. These structural changes are more pronounced for the light rare earths than for heavy ones, also reflected in the significant change of the DOS in the vicinity of E_f of the former. This DOS behavior is connected with the only free internal structural parameters in these compounds, the z_B position of boron, and the c/a ratio of the lattice constants. Thus, we calculated the forces on the boron atoms at the experimental boron position for the whole series of compounds and found in all cases only a small force of about -15 mRy/a.u. Optimization of this parameter in the Y and La compound shows that relaxing such forces corresponds to a negligible small shift of z_B of about -0.1% and thus the theoretical equilibrium is in all cases very close to the experiment.

To investigate the influence of the lattice parameters a and c, we calculated the total energy as a function of the c/a ratio for $\mathrm{YNi_2B_2C}$ and $\mathrm{LaNi_2B_2C}$. In these sets of calculations the z_B parameter was constrained to the value obtained from the force minimization. As shown in Fig. 4 the total energy depends sensitively upon the c/a ratio and exhibits a pronounced minimum close to the experimental c/a value[31] indicated by the dashed line. This property of the total energy is associated with the strong covalent bonding within both the C-B-C chains and the B-Ni-B tetrahedral network. As the C-B and Ni-B distances are very rigid the total energy is minimized through the simultaneous change of the lattice parameters a and c. The c/a ratios that minimize the total energy for $\mathrm{YNi_2B_2C}$ (c/a=2.959) and for $\mathrm{LaNi_2B_2C}$ (c/a=2.586) are in good agreement with the experimental results of Siegrist *et al.*[31] (dashed lines in Fig. 4). We analyzed the total DOS for the set of c/a values used in the total energy calculations and found that both the value of $N(E_f)$ and the shape of total DOS near E_f strongly depend on the particular

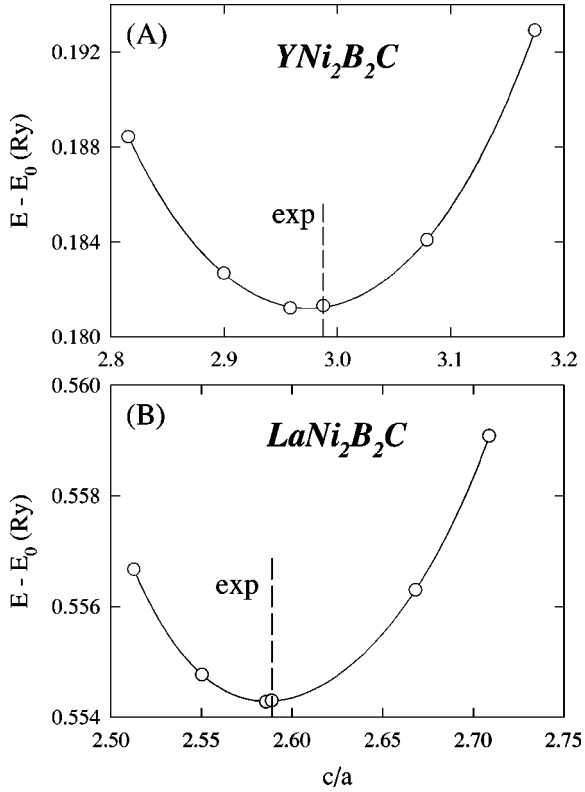

FIG. 4. The calculated DFT total energy as a function of the c/a ratio for YNi_2B_2C (A) and $LaNi_2B_2C$ (B). The experimental c/a ratio is denoted by the vertical dashed line. $E_0=-13\,012$ Ry and $E_0=-23\,231$ Ry are used for YNi_2B_2C (A) and $LaNi_2B_2C$ (B), respectively. The full line is a guide for the eye.

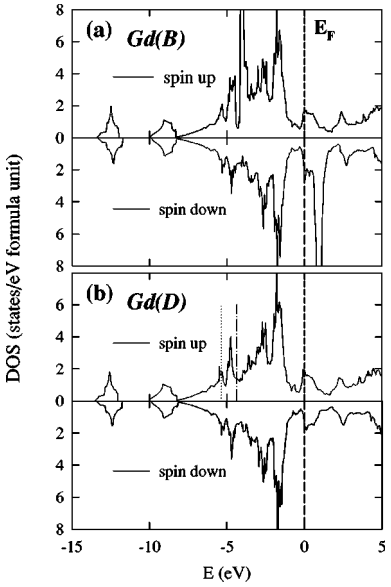

FIG. 5. Total spin-up and spin-down DOS of $GdNi_2B_2C$. The labels (a) and (b) denote the Gd(B) and Gd(D) model for the $4f$ states, respectively. The energy levels of the fully occupied localized $4f_{5/2}$ and $4f_{7/2}$ spin-up states are indicated by a dotted and dashed-dotted vertical line, respectively. The empty localized $4f_{5/2}$ and $4f_{7/2}$ spin-down states are not shown.

value of c/a. For example, in the case of $LaNi_2B_2C$ the total DOS calculated for $c/a=2.958$ is very similar to the one presented by Mattheiss *et al.*[16] for the ''ideal crystal structure'' with the optimal B-Ni-B angle of 109°. However, this c/a ratio corresponds to a total energy that is about 38 mRy higher than that calculated for the minimal energy (or experimental) $c/a=2.589$ ratio of $LaNi_2B_2C$. Thus, our investigations indicate a high sensitivity of both $N(E_f)$ and the shape of the total DOS around E_f. It also demonstrates that DFT calculations allow us to predict from first principles (i.e., without knowing the experimental structural parameters) whether or not a peak in the DOS appears in the vicinity of E_f, a feature that seems to be a necessary condition for the occurrence of superconductivity in these compounds.

To test the possible impact of the treatment of the localized and highly correlated $4f$ states upon the calculated DOS, we also performed DOS calculations using the schemes denoted Gd(B)–Gd(E) and Tb(B)–Tb(D) (see Sec. II B). For Gd(B), Gd(C), and Gd(E) where $4f$ states are treated as band states, we found moderately enhanced DOS at the Fermi level (see Table II) with respect to Gd(A) ranging from 3.81 states/eV for Gd(C) to 4.02 states/eV for Gd(B). The DOS curves for the spin-polarized LSDA cases Gd(B) and Gd(D) are shown in Fig. 5. The overall shape of all DOS curves is similar to the nonspinpolarized case Gd(A) shown in Fig. 3. The only difference is associated with the two spikes at -4 eV [$4f$ spin-up states, Fig. 5(a)] and at 0.8 eV [$4f$ spin-down states, Fig. 5(a)]. The calculated DOS for Gd(D) is depicted in Fig. 5(b), where the energy levels of the $4f_{5/2}$ and $4f_{7/2}$ localized spin-up states

TABLE II. Site projected partial charges Q_i (in electrons) of the valence states inside Gd and Tb atomic spheres, the total DOS $N(E_F)$, and the valence and core spin magnetic moments in μ_B. The symbols Gd(B)–Gd(E), Tb(B)–Tb(D) denote the method of treating the $4f$ states and the chosen DFT potential (see Sec. II C).

	Gd(B)	Gd(C)	Gd(D)	Gd(E)	Tb(B)	Tb(C)	Tb(D)
$Q_s(R)$	2.147	2.143	2.151	2.143	2.166	2.163	2.167
$Q_p(R)$	6.016	6.018	6.027	6.013	6.062	6.068	6.063
$Q_d(R)$	0.910	0.897	0.995	0.899	1.010	0.993	1.015
$Q_f(R)$	7.136	7.124	0.077	7.128	0.079	0.077	0.077
$N(E_F)$	4.03	3.81	3.41	4.01	3.52	4.13	3.85
M_S(valence)	6.917	6.938	0.149	6.893	0.124		
M_S(core)	0.0	0.0	7.0	0.0	6.0		

TABLE III. Data for $R\mathrm{Ni}_2\mathrm{B}_2\mathrm{C}$ as in Table I but with R=La, Pr, Nd, Sm, Gd, Tb. The symbols Gd(A) and Tb(A) denote the method of treating the $4f$ states (see Sec. II C).

	La	Pr	Nd	Sm	Gd(A)	Tb(A)
$Q_s(R)$	2.055	2.087	2.102	2.127	2.152	2.167
$Q_p(R)$	5.709	5.836	5.885	5.965	6.032	6.067
$Q_d(R)$	0.877	0.941	0.964	0.981	0.995	1.014
$Q_f(R)$	0.071	0.074	0.074	0.074	0.074	0.076
Q_s(Ni)	0.454	0.460	0.463	0.462	0.463	0.468
Q_p(Ni)	6.434	6.458	6.469	6.476	6.485	6.499
Q_d(Ni)	8.356	8.338	8.338	8.322	8.315	8.314
Q_f(Ni)	0.020	0.022	0.023	0.024	0.024	0.026
$N(E_F)$	2.30	2.00	2.10	2.97	3.57	4.11
$N_R(E_F)$	0.23	0.20	0.22	0.32	0.38	0.41
$N_{Ni}(E_F)$	1.34	1.26	1.28	1.76	2.12	2.52
$N_B(E_F)$	0.11	0.09	0.10	0.14	0.18	0.21
$N_C(E_F)$	0.06	0.04	0.04	0.07	0.09	0.10
$N_I(E_F)$	0.56	0.41	0.46	0.68	0.80	0.87

occur at -5.38 eV and -4.65 eV below E_f, respectively. The DOS in the vicinity of E_f(-0.5 to 0.5 eV) is quite similar in all cases Gd(A)–Gd(E). The marginal enhancement of $N(E_f)$ for Gd(B), Gd(C), and Gd(E) originates from the tail of the $4f$ spin-down states as it was also found for elemental Gd metal.[37] This conjecture is also supported by the fact that a similar systematic $N(E_f)$ enhancement is not observed for Tb(B)–Tb(D) where the $4f$ states are treated as open core states (see Table II). The variation of $N(E_f)$ for Tb(B)–Tb(D) amounts to about 15% indicating that $N(E_f)$ depends only slightly on the particular V_{exc} potential (LDA, LSDA, or GGA) used in our DFT calculations.

Spin magnetic moments obtained from our spin polarized calculations [see Table II, schemes Gd(B)–Gd(E)] are reasonably close to the experimental value[5] of $7\mu_B$. Using the self-consistent charge density obtained including spin-orbit coupling [scheme Gd(E)] we also calculated the orbital magnetic moment $M_L=0.05\mu_B$ at the Gd site. This value is of similar size as was found for elemental Gd metal.[35,37] No significant magnetic moment was found on the Ni site ($M_S^{\mathrm{Ni}}<0.05\mu_B$) in R=Gd, Tb materials in agreement with neutron diffraction studies.[5]

The cohesive properties such as equilibrium volume and c/a ratio also depend on the different way of treating the $4f$ electrons in $\mathrm{GdNi}_2\mathrm{B}_2\mathrm{C}$. We have done both a nonspin polarized calculation ($4f$ electrons itinerant) yielding an optimal c/a value of 2.898 and the scheme Gd(B) (spin polarized calculations with $4f$ electrons itinerant) leading to 2.886, values that are both close to the experimental ratio of $c/a=2.896$. Similar good agreement was found for $\mathrm{YNi}_2\mathrm{B}_2\mathrm{C}$ and $\mathrm{LaNi}_2\mathrm{B}_2\mathrm{C}$ (see Fig. 4). The EFG values, however, are more sensitive to the treatment of the f states, since, for example, the Gd-EFG was found to be 15.06×10^{21} V m^{-2} and 12.89×10^{21} V m^{-2} in the two calculations mentioned above, nonspin polarized or Gd(B) scheme. Since the former value is more than 20% larger than the experimental value[45] of 12.1×10^{21} V m^{-2}, scheme Gd(B) is clearly better. Therefore, the EFG at the Gd site is a more sensitive quantity than the equilibrium volume, c/a ratio, and magnetic moments, in order to investigate the localized or itinerant nature of the $4f$ states in such systems.

B. The relation between $N(E_f)$ and the superconducting transition temperature T_c

The systematic electronic structure calculations presented in the previous subsection revealed a significant reduction of the electronic DOS at the Fermi level $N(E_f)$ on the light-rare-earth side of the $R\mathrm{Ni}_2\mathrm{B}_2\mathrm{C}$ series (see Table III). A reduction of $N(E_f)$ of $\mathrm{YNi}_2\mathrm{B}_2\mathrm{C}$ was also observed upon Ni/Co substitution deduced from experiment[49] as well as theoretical studies.[13] Accordingly, T_c of $\mathrm{Y(Ni}_{1-x}\mathrm{Co}_x)_2\mathrm{B}_2\mathrm{C}$ drops rapidly with $dT_c/dx\sim-100$ K for $x\leqslant0.1$ (see Ref. 50). Using the McMillan formula[51] it could be shown that the decrease of $N(E_f)$ is accompanied by a proportional reduction of the electron-phonon mass enhancement $\lambda=N(E_f)\langle I^2\rangle/M\langle\omega^2\rangle$ in $\mathrm{Y(Ni}_{1-x}\mathrm{Co}_x)_2\mathrm{B}_2\mathrm{C}$ and also the related system $\mathrm{La}_3(\mathrm{Ni}_{1-x}\mathrm{Co}_x)_2\mathrm{B}_2\mathrm{N}_{3-\delta}$ while the average electron-phonon matrix element $\langle I^2\rangle$, the characteristic phonon frequency $\langle\omega^2\rangle$, and the mean atomic mass M were found to stay rather constant for Ni/Co substitution.[52] By analogy we expect also for the $R\mathrm{Ni}_2\mathrm{B}_2\mathrm{C}$ series that the λ value will decrease roughly proportional to the drop of $N(E_f)$ on the light-rare-earth side. As the logarithmic and second moments of the phonon spectra, $\omega_{\ln}$ and $\overline{\omega}_2$, of $\mathrm{LaNi}_2\mathrm{B}_2\mathrm{C}$ and $\mathrm{LuNi}_2\mathrm{B}_2\mathrm{C}$ are rather close to each other[19] their variation along the $R\mathrm{Ni}_2\mathrm{B}_2\mathrm{C}$ series is relatively small compared to the significant drop of $N(E_f)$ revealed by the band structure results. Thus, for a first approximation the electron-phonon mass enhancement λ^R of $R\mathrm{Ni}_2\mathrm{B}_2\mathrm{C}$ is estimated by rescaling λ^{Lu} of $\mathrm{LuNi}_2\mathrm{B}_2\mathrm{C}$ by $\lambda^R_{N(E_f)}=\lambda^{\mathrm{Lu}}\times N(E_f)^R/N(E_f)^{\mathrm{Lu}}$ with $\lambda^{\mathrm{Lu}}=1.15$ given in Ref. 19 [the superscript R marks the $R\mathrm{Ni}_2\mathrm{B}_2\mathrm{C}$ compound to which the $N(E_f)$ or λ values belong, while the subscripts $\alpha=R$, Ni, B, C used below indicate atom or site projected quantities]. Accordingly, the superconducting transition temperature expected in the absence of magnetic pair breaking, T_{c0}, is roughly given by the

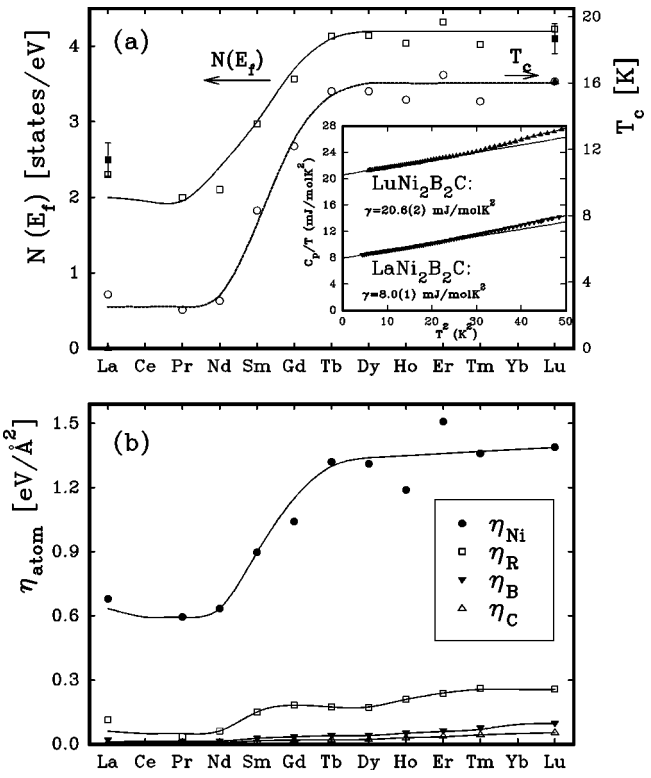

FIG. 6. The calculated $N(E_f)$ and the superconducting transition temperatures T_{c0}^R rescaled according to the McMillan formula (see text) of the $R\mathrm{Ni}_2\mathrm{B}_2\mathrm{C}$ series. Full squares: experimental $N(E_f)$ values for $R=$La and Lu from the electronic specific heat coefficient γ derived from the linear low-temperature extrapolation of C_p/T versus T^2 shown in the inset (see text). Full triangles: experimental T_c values for $\mathrm{LaNi}_2\mathrm{B}_2\mathrm{C}$ and $\mathrm{LuNi}_2\mathrm{B}_2\mathrm{C}$ (a); the Hopfield parameters η_α obtained by the RMTA approach; the full lines are guides for the eye (b).

McMillan relation[51] $T_{c0}^R \propto \exp\{-1.04[1+\lambda^R]/(\lambda^R-\mu^*[1+0.62\lambda^R])\}$. The T_{c0}^R values of $R\mathrm{Ni}_2\mathrm{B}_2\mathrm{C}$ obtained by this simple approach (using a constant prefactor and $\mu^* \simeq 0.13$) are shown in Fig. 6(a) together with the $N(E_f)$ values. While $N(E_f)$ and accordingly T_{c0} remain fairly constant on the heavy-rare-earth side ($R=$Tb, . . . ,Lu), the reduction of the density of states $N(E_f)$ on the light-rare-earth side is large enough to explain the suppression of superconductivity to below 3 K for $\mathrm{LaNi}_2\mathrm{B}_2\mathrm{C}$, to below $T_N=4.0$ K and 4.8 K for $\mathrm{PrNi}_2\mathrm{B}_2\mathrm{C}$ and $\mathrm{NdNi}_2\mathrm{B}_2\mathrm{C}$, respectively. We note that the formation of the antiferromagnetic ground state (not considered in our calculations) may influence the electronic structure *below* T_N.

In order to demonstrate that the lower $N(E_f)$ of $\mathrm{LaNi}_2\mathrm{B}_2\mathrm{C}$ with respect to $\mathrm{LuNi}_2\mathrm{B}_2\mathrm{C}$ is well supported by the experiment, we include in Fig. 6(a) the values of $N(E_f)=3\gamma/[(\pi k_B)^2(1+\lambda)]$ (full squares) obtained from the normal state specific heat displayed in the inset as C/T vs T^2 yielding the Sommerfeld values $\gamma=8.0(1)$ and 20.6(2) mJ/mol K^2 for $\mathrm{LaNi}_2\mathrm{B}_2\mathrm{C}$ and $\mathrm{LuNi}_2\mathrm{B}_2\mathrm{C}$, respectively.[55] The fact that $\mathrm{LaNi}_2\mathrm{B}_2\mathrm{C}$ is not superconducting above 20 mK (see Ref. 7) provides an upper limit for the electron-phonon enhancement $\lambda^{\mathrm{La}} \leqslant 0.35$ according to the McMillan relation, which is significantly smaller than the rescaled value $\lambda^{\mathrm{La}}_{N(E_f)}=0.65$ obtained above. With $\lambda^{\mathrm{Lu}}=1.15$ and $\lambda^{\mathrm{La}} \sim 0.35$ deduced from T_c and the experimental γ values we obtain $N(E_f)^{\mathrm{Lu}}=4.06$ and $N(E_f)^{\mathrm{La}}=2.51$ states/eV which are in good agreement with those calculated *ab initio*.

The significant difference between the rescaled value $\lambda^{\mathrm{La}}_{N(E_f)}=0.65$ and the upper limit given by the experiment $\lambda^{\mathrm{La}} \leqslant 0.35$ implies that not only $N(E_f)$ drops but concomitantly the electron-phonon matrix element $\langle I^2 \rangle$, is reduced due to changes of the band structure in the light-rare-earth borocarbides. Thus, we implemented the calculation of the matrix elements $\langle I^2 \rangle$ into the WIEN97 code using an approach based on the rigid muffin-tin approximation (RMTA).[53,54] Such calculations were reported for $\mathrm{YNi}_2\mathrm{B}_2\mathrm{C}$ by Lee *et al.*[12] and for $\mathrm{LuNi}_2\mathrm{B}_2\mathrm{C}$ by Pickett and Singh[18] yielding $\lambda \sim 0.6$ and $\lambda \sim 2.6$, respectively, and these values were confirmed by our independent calculations based on the WIEN97 code [when using the same values for the Debye temperature Θ_D and an average density of states $N(E_f)$]. Since the experimental λ values of $\mathrm{YNi}_2\mathrm{B}_2\mathrm{C}$ and $\mathrm{LuNi}_2\mathrm{B}_2\mathrm{C}$ are both close to one,[19] the large discrepancy between the experimental and theoretical λ values may be attributed to the substantial approximations introduced by the RMTA approach to calculate the mean electron-phonon matrix elements of the individual atoms $\langle I_\alpha^2 \rangle$ ($\alpha=R$, Ni, B, C). Moreover it has to be noted that a further severe approximation occurs when summing over the atoms of a multicomponent compound to calculate

$$\lambda = \sum_\alpha \frac{N(E_f)\langle I_\alpha^2 \rangle}{M_\alpha \langle \omega^2 \rangle}, \tag{6}$$

where $\langle \omega^2 \rangle = \Theta_D^2/2$ is usually estimated from the Debye temperature. Thereby, the factor $1/M_\alpha$ strongly weights the light atoms (boron and carbon) while the rare-earth contribution becomes negligible. However, from INS experiments[22,23] it is known that in particular those low-energy modes ($\sim$10–15 meV) that originate from the rare-earth motion within the rigid cage formed by Ni, B, and C couple to the electronic system, in particular to a nesting feature at the Fermi surface. The B and C modes, on the other hand, are rather high in energy (major spectral weights at 50, 100, 160 meV) and thus are hardly relevant for the electron phonon coupling.[23] As ω enters quadratically into Eq. (6), it is obvious that the assumptions on $\langle \omega_\alpha^2 \rangle$ are crucial for the absolute value derived for λ.

For multicomponent compounds an important point is the calculation of the Hopfield parameters $\eta_\alpha = N(E_f)\langle I_\alpha^2 \rangle$ where in some papers[12,18] an average density of states $N(E_f)$ for all atoms is used, while in others (see, e.g., Ref. 54) the site projected density of states is assumed to be the relevant one, i.e., $\eta_\alpha = N_\alpha(E_f)\langle I_\alpha^2 \rangle$. For the borocarbides $N_\alpha(E_f)$ values are summarized in Table I and show, for example, for $\mathrm{LuNi}_2\mathrm{B}_2\mathrm{C}$ that the Ni site DOS $N_{\mathrm{Ni}}(E_f) \simeq 2.3$ is largest while $N_{\mathrm{Lu}}(E_f) \simeq 0.4$, $N_{\mathrm{B}}(E_f) \simeq 0.25$, and $N_{\mathrm{C}}(E_f) \simeq 0.15$ are comparably small. The remaining 0.96 states/eV f.u. correspond to the plane-wave contribution from the interstital region. Using these site projected DOS for the Hopfield parameters, we obtain $\eta_{\mathrm{Ni}} = N_{\mathrm{Ni}}(E_f)\langle I_{\mathrm{Ni}}^2 \rangle = 1.42$ eV/Å^2, which is significantly larger than $\eta_{\mathrm{Lu}} = N_{\mathrm{Lu}}(E_f)\langle I_{\mathrm{Lu}}^2 \rangle = 0.26$ eV/Å^2, $\eta_{\mathrm{B}} = N_{\mathrm{B}}(E_f)\langle I_{\mathrm{B}}^2 \rangle = 0.1$ eV/Å^2, and $\eta_{\mathrm{C}} = N_{\mathrm{C}}(E_f)\langle I_{\mathrm{C}}^2 \rangle = 0.06$ eV/Å^2. With $\langle \omega^2 \rangle = 1.1 \times 10^{27}$ s^{-2} (estimated from

$\Theta_D = 360$ K) these values yield $\lambda \simeq 0.4$ compared to $\lambda \simeq 0.9$ obtained via $\eta_\alpha = N(E_f)\langle I_\alpha^2 \rangle$ with an average DOS $N(E_f) \simeq 0.7$ states/eV atom. The fact that $\lambda \simeq 0.9$ is close to the experimental result may suggest that the average DOS is the appropriate choice for calculating the η values. However, calculating $\lambda = \Sigma N(E_f)_\alpha \langle I_\alpha^2 \rangle / M_\alpha \langle \omega_\alpha^2 \rangle$ with more realistic mean frequencies ω_α for each atom sort, e.g., ω_{Lu} corresponding to 10 meV and $\omega_{\mathrm{Ni}} \sim 22$ meV (suggested by the Born–von Karman calculations by Gompf *et al.*,[23] see Fig. 6 therein) one can easily obtain a λ value close to one.

The RMTA approach yields, irrespective of the uncertainty of the absolute value of λ, information about the variation of the Hopfield parameters η_α across the $R\mathrm{Ni_2B_2C}$ series that at least gives a qualitative argument for the applicability of the very simple rescaling of T_{c0} shown in Fig. 6(a) where we took into account only the changes of $N(E_f)$. In Fig. 6(b) we show for comparison the RMTA results for $\eta_\alpha = N(E_f)_\alpha \langle I_\alpha^2 \rangle$. The obvious correlation between the variation of $N(E_f)$ and the η_α values is connected with the fact that the calculated site projected contributions $N_\alpha(E_f)$ follow the trend of the total $N(E_f)$ going from heavy-rare-earth borocarbides to the light ones (see Tables I and II).

Hence, we conclude that magnetic pair-breaking is the source for the suppression of superconductivity in $\mathrm{GdNi_2B_2C}$ and $\mathrm{TbNi_2B_2C}$ due to the large de Gennes factor $(g-1)^2 J(J+1)$ because $N(E_f)$ is of the same magnitude as for the corresponding Lu and Y compound. On the other hand, the reduction of $N(E_f)$ and λ appears to be detrimental for the occurrence of superconductivity in $\mathrm{PrNi_2B_2C}$ and $\mathrm{NdNi_2B_2C}$ where the pair breaking is weak due to the small de Gennes factor. $\mathrm{SmNi_2B_2C}$ seems to be a borderline case where the absence of superconductivity may be attributed to the reduction of $N(E_f)$ as well as the influence of magnetism.

This conclusion is in contrast to the suggestion by Pellegrin *et al.*[27] drawn from their Ni L and B K near x-ray absorption spectra of polycrystalline $R\mathrm{Ni_2B_2C}$ ($R = Y$, Sm, Tb, Ho, Er, Tm, Lu). According to their near-edge x-ray-absorption fine structure data there is no significant variation of the Ni $3d$ and a slight reduction of the B $2p$ projected DOS at or close to E_f in the $R\mathrm{Ni_2B_2C}$ series. From these results the authors deduce that the decrease of T_c in the earlier rare-earth compounds of this series is not related to the position of the Fermi level relative to a maximum or to a decrease of the DOS at or close to E_f. Our calculated charges inside the Ni atomic sphere (see Tables I, III) are almost constant through the whole series. For this charge analysis the constraint muffin-tin radius $R_{MT} = 2.25$ a.u. was used for Ni. Nevertheless, the total DOS at or close to the Fermi level drops significantly in the series from Gd via Sm, Nd, and Pr to La but remains rather constant for $R = Y$, Tb, Dy, Ho, Er, Tm (see Figs 2, 3, and 6 and Tables I – III). The changes in the DOS are, however, more pronounced below E_f in the occupied region of the valence states and thus are not accessible to the x-ray absorption spectra. We emphasize that the calculated values of the B-DOS $N_B(E_F)$ decrease for the rare earths lighter than Gd (see Tables I and III), a fact that is in agreement with the changes near the absorption boron K threshold observed experimentally.[27] Therefore, we cannot support the conclusion by Pellegrin *et al.*[27] mentioned above but propose that the disappearance of superconductivity in the light-rare-earth borocarbides is caused by the reduction of $N(E_f)$. The same conclusion was also proposed by a recent photoemission and theoretical investigation of $\mathrm{YNi_2B_2C}$.[15]

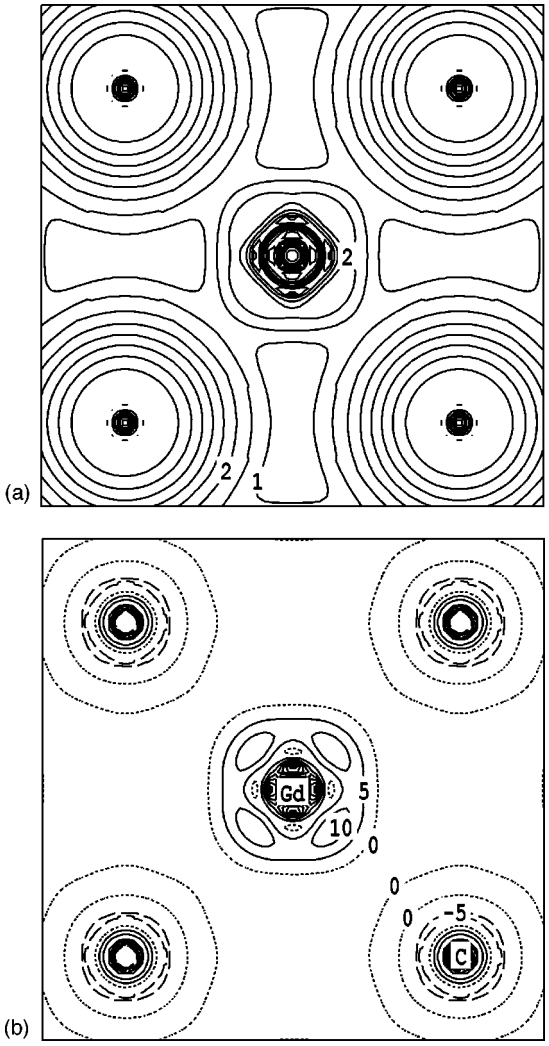

FIG. 7. Charge density for $\mathrm{GdNi_2B_2C}$ in the (001) plane. (*A*) Valence density (contour levels start at $0.1e/\text{Å}^3$, and increase by a factor of $\sqrt{2}$). (*B*) Difference density taken between the crystalline and the superposed atomic density (contour levels with an increment of $0.05e/\text{Å}^3$, negative density denoted by dashed lines).

C. Valence charge density and electric-field gradients

The valence charge density (omitting the Gd $5p$ electron density) and the respective difference density $\Delta\rho$ (difference between crystalline density and a superposition of free atomic densities) of $\mathrm{GdNi_2B_2C}$ is shown in the (001) [Figs. 7(a,b)] and the (100) plane [Figs. 8(a,b)]. From Figs. 7(a) and 7(b) it is obvious that the charge density is essentially spherical around the C atoms but the Gd charge density exhibits significant differences from spherical symmetry displaying a fourfold rotational symmetry in some region close to the Gd nuclei. While the bonding between Gd and C is dominated by ionic contributions, additional quite large aspherical distortions occur in the regions close to the Gd sites

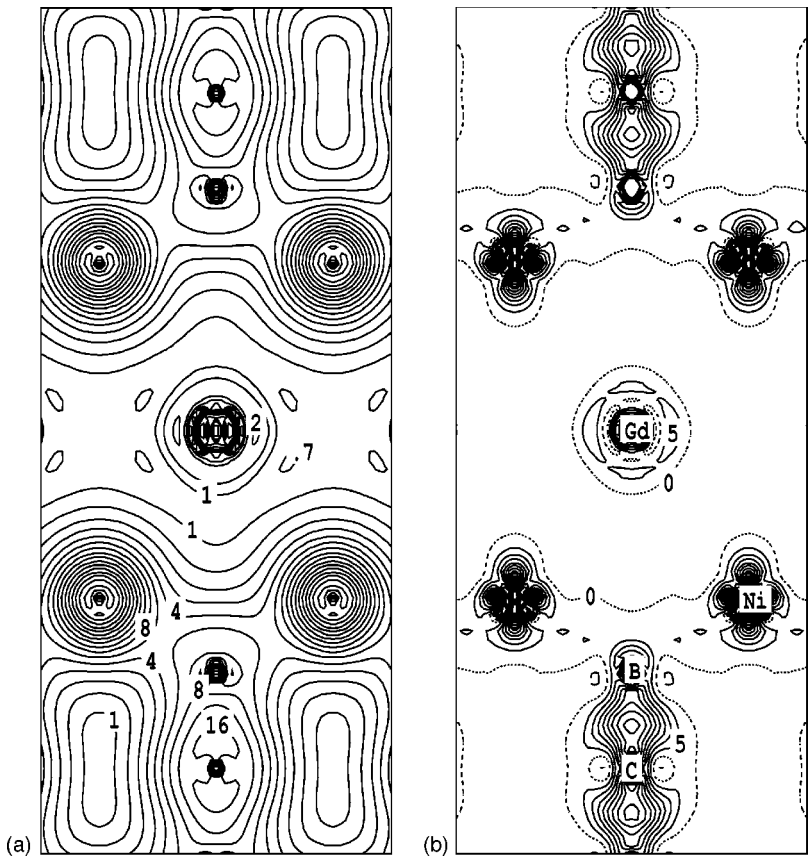

FIG. 8. Charge density for $GdNi_2B_2C$ in the (100) plane. Details as in Fig. 7.

presenting covalent contributions. In contrast to the (001) plane the valence charge density in the (100) plane [Fig. 8(a)] shows much smaller departures from spherical symmetry around the Gd atom as can also be seen in the difference density $\Delta\rho$ [Fig. 8(b)] where only two very weak positive maxima in the (010) direction occur. These significant asymmetries of the valence charge density in the region close to the R nuclei are the origin of the quite large value of the EFG at the Gd site. Also the crystal field (CF) interaction of the localized $4f$ states is strongly influenced by this on-site asphericity. Besides these features related to the R atom, Fig. 8(b) nicely manifests the strong directional bonding between boron and carbon atoms connecting the two Ni-B layers and the covalent character of the bonding between nickel and boron. We can conclude that the valence charge density in the neighborhood of the localized $4f$ density (up to the fourth C nearest neighbors) is quite inhomogeneous and exhibits significant anisotropic features. Therefore, one can expect a remarkable anisotropy of magnetic properties originating from CF interaction of $4f$ electrons in question. This will be addressed in detail in another paper.[56]

The EFG's at all atomic positions of $GdNi_2B_2C$ are summarized in Table IV for all constrained DFT calculations Gd(A)–Gd(E) (see Sec. II C). The theoretical EFG at Gd reveals good agreement between theory and experiment.[45] The ferromagnetic calculations Gd(B) and Gd(D) provide poorer agreement than the others. The calculated value of the EFG does not change significantly when spin-orbit coupling is included in the calculations [see Gd(E)]. The experimental value of the Gd EFG in $GdNi_2B_2C$ is much larger than in $GdNi_2Si_2(-1.2\times10^{21}\ \mathrm{V\,m^{-2}})$,[57] which has the $ThCr_2Si_2$ crystal structure. This structural type is closely related to the crystal structure of the RNi_2B_2C compounds (both have the space group $I4/mmm$), but the additional C atoms close to the R site increase the EFG significantly due to the covalent R-C interactions mentioned above. The existence of large EFG values is of great importance in connection with the anisotropy in the magnetic properties of RNi_2B_2C.

In order to analyze the origin of the Gd-EFG, we decompose the calculated Gd-EFG [Gd(B)] into several different contributions (Table V). The lattice contribution (the contribution to the EFG from outside the respective atomic sphere) is negligibly small ($10^{20}\ \mathrm{V\,m^{-2}}$ or less than 1% of the EFG), which reflects the fact that the physical origin of the EFG lies in the deviation from spherical symmetry of the valence charge density near the Gd nucleus. This aspherical charge density can be resolved into l-l' contributions for

TABLE IV. Electric field gradients (EFG) of $GdNi_2B_2C$ (in $10^{21}\ \mathrm{V\,m^{-2}}$) at all nuclear sites. The symbols Gd(A)–Gd(E) denote the method of treating the $4f$ states and the selected DFT potential (see Sec. II C). The experimental data are taken from Ref. 45.

EFG	Gd	Ni	B	C
Gd(A)	12.10	2.44	1.44	2.65
Gd(B)	12.89	2.48	1.39	2.39
Gd(C)	12.05	2.23	1.33	2.22
Gd(D)	12.36	2.24	1.45	2.66
Gd(E)	12.17	2.21	1.33	2.24
Experiment	12.1			

TABLE V. EFG analysis for the Gd site in $GdNi_2B_2C$ [calculation Gd(B), see Sec. II C]. The on-site contribution is analyzed in terms of s-d ($5s$ and $6s$), p-p ($5p$ and $6p$), d-d($5d$), and f-f($4f$) valence electron contributions. The lattice contribution includes everything from outside the Gd sphere.

Gd(B)	On-site	Lattice	Total
s-d	0.11		
$5p$-$5p$	−30.63		
$6p$-$6p$	43.80		
d-d	−0.15		
f-f	−0.10		
Others	−0.01		
	13.02	−0.13	12.89

each spin direction as shown in Sec. II D. The dominant contribution to the EFG comes from the asphericity of Gd $5p$ and $6p$ electrons inside the atomic sphere. We found that the low-lying $5p$ states contribute with a large negative portion to the EFG, which is compensated by an even larger positive $6p$ contribution. Thus, the final EFG stems from a delicate balance of the $5p$ and $6p$ anisotropy. This is in contrast to Coehoorn,[17] who has neglected the contribution from the $5p$ states and has taken into account only the on-site asphericity of the charge density related to $6p$ and $5d$ electrons. Nevertheless, he has found a reasonable value for the EFG $=12.8\times10^{21}$ V m^{-2} using the ASW method in the ASA approximation. The large positive value of the EFG indicates that the occupation of orbitals within the Gd-C layers (p_x and p_y) is larger ($n_{p_x}=n_{p_y}=0.134$) than perpendicular to it ($n_{p_z}=0.081$). Small f-f, s-d, and d-d contributions, all with comparable magnitude, are also present. Using the decomposition of the charge density coefficient ρ_{20} [see Eq. (2)] we have calculated the partial contributions from each ($l=l'=3$, $m=m'=3,1,0$) of the occupied orbitals. We found that the partial contributions of the occupied $4f$ spin up states can reach about 10% of the related p-p partial contributions but the final value of $EFG_{f\text{-}f}$ is quite small due to an almost complete cancellation. Thus, the EFG proofs that the $4f$ states are effectively almost spherical as one would expect in this case.

YNi_2B_2C single crystals have also been investigated by ^{11}B nuclear magnetic resonance[58,59] and the measured quadrupole frequency was found to be constant from 300 K down to 15 K. The corresponding EFG, 1.42×10^{21} V/m^2, is in very good agreement with our value of 1.4×10^{21} V/m^2 calculated for YNi_2B_2C. This calculated B-EFG is almost constant for all RNi_2B_2C compounds as was also experimentally observed by Ikushima *et al.*[60] who obtained 1.48×10^{21} V/m^2 for the B-EFG for $LuNi_2B_2C$.

We have not found any direct experimental EFG measurements on the Ni site, but ^{57}Fe Mössbauer spectroscopy[61] on a substituted Ni site provides a quadrupole splitting of $\Delta E_Q=0.27$ mm/s. Using the value of 0.16 b for the ^{57}Fe nuclear quadrupole moment,[62] we can estimate the EFG at that site to be about 2.4×10^{21} V m^{-2}, which compares reasonably well with our calculated values for the regular Ni site quoted in Table IV.

IV. CONCLUSIONS

The calculations based on the DFT theory are able to provide useful information about the electronic structure of rare-earth borocarbides RNi_2B_2C. The calculations of the electronic structure yield the DOS, which shows the Fermi energy located in the DOS peak for $R=$ Y, Dy, Ho, Er, Tm, and Lu. In the sequence of $R=$ Tb, Gd, and Sm, this peak is gradually broadened and in the case of $R=$ Pr, Nd, and La, the Fermi energy is situated in a broad valley of the DOS. We verified that these general trends do not depend on the details (LSDA, GGA, spin orbit) of the DFT methods used. The calculated reduction of the density of states $N(E_f)$ on the light-rare-earth side (in particular for $R=$ La, Pr, and Nd) is large enough to explain the suppression of superconductivity to below 3 K for Nd, Pr, and La. The calculation of the Hopfield parameters confirms this conclusion. Furthermore, there is good agreement between the calculated and experimental $N(E_f)$ of YNi_2B_2C, $LaNi_2B_2C$, and $LuNi_2B_2C$. This consistent physical picture is only reached when we assume that the $4f$ electrons in $R=$ Pr, Nd, Sm, Tb, Dy, Ho, Er, and Tm are atomiclike (localized) and thus no $4f$ projected DOS is present at E_f. In contrast to those compounds, $GdNi_2B_2C$ and $LuNi_2B_2C$ show according to our analysis that $N(E_f)$ and related properties are not substantially influenced by the itinerant or localized treatment of the $4f$ states used in this work (see Sec. II C). The EFG on the crystallographic sites of $GdNi_2B_2C$ and YNi_2B_2C were calculated and the values found for the Gd site and B site are in good agreement with experimental data. The relatively large EFG on the Gd site originates from a strong cancellation between positive $6p$-$6p$ and negative $5p$-$5p$ contributions.

ACKNOWLEDGMENTS

The work in Vienna was partly supported by the Austrian Science Foundation (M.D., Grant No. M 00413-PHY), project by G.H. Grant No. P 11090, and OEAD project WTZ 1999/21. The work of M.D. and S.K. done at Prague was supported by the Grant Agency of Czech Republic under Grants Nos. 202/00/1602, 202/99/0184, and 106/98/0507, respectively.

[1] R. Nagarajan, C. Mazumdar, Z. Hossain, S.K. Dhar, K.V. Gopalakrishnan, L.C. Gupta, C. Godart, B.D. Padalia, and R. Vijayaraghavan, Phys. Rev. Lett. **72**, 274 (1994).

[2] R.J. Cava, H. Takagi, H.W. Zandbergen, J.J. Krajewski, W.F. Peck, Jr., T. Siegrist, B. Batlogg, R.B. van Dover, R.J. Felder, K. Mizuhashi, J.O. Lee, H. Eisaki, and S. Uchida, Nature (London) **367**, 254 (1994).

[3] T. Siegrist, H.W. Zandbergen, R.J. Cava, J.J. Krajewski, and W.F. Peck, Jr., Nature (London) **367**, 146 (1994).

[4] H. Eisaki, H. Takagi, R.J. Cava, B. Batlogg, J.J. Krajewski, F.W. Peck, K. Mizuhashi, J.O. Lee, and S. Uchida, Phys. Rev. B **50**, R647 (1994).

[5] J.W. Lynn, S. Skanthakumar, Q. Huang, S.K. Sinha, Z. Hossain, L.C. Gupta, R. Nagarajan, and C. Godart, Phys. Rev. B **55**, 6584

(1997).
[6] E. Alleno, Z. Hossain, R. Nagarajan, and L.C. Gupta, Phys. Rev. B **52**, 7428 (1995).
[7] M. El Massalami, R.E. Rapp, and G.J. Nieuwenhus, Physica C **304**, 184 (1998).
[8] A. Yatskar, N.K. Budraa, W.P. Beyermann, P.C. Canfield, and S.L. Bud'ko, Phys. Rev. B **54**, R3772 (1996).
[9] S.K. Dhar, R. Nagarajan, Z. Hossein, E. Tominez, C. Godart, L.C. Gupta, and R. Vijayaraghavan, Solid State Commun. **98**, 985 (1996).
[10] G. Hilscher and H. Michor, in *Studies on High Temperature Superconductors*, edited by A.V. Narlikar (Nova, New York, 1999), Vol. 28, p. 241.
[11] D.J. Singh, Solid State Commun. **98**, 899 (1996).
[12] J.I. Lee, T.S. Zhao, I.G. Kim, B.I. Min, and S.J. Youn, Phys. Rev. B **50**, 4030 (1994).
[13] P. Ravindran, B. Johansson, and O. Eriksson, Phys. Rev. B **58**, 3381 (1998).
[14] L.F. Mattheiss, Phys. Rev. B **49**, 13 279 (1994).
[15] H. von Lips, Z. Hu, C. Grazioli, S.-L. Drechsler, G. Behr, M. Knupfer, M.S. Golden, J. Fink, H. Rosner, and G. Kaindl, Phys. Rev. B **60**, 11 444 (1999).
[16] L.F. Mattheiss, T. Siegrist, and R.J. Cava, Solid State Commun. **91**, 587 (1994).
[17] R. Coehoorn, Physica C **228**, 331 (1994).
[18] W.E. Pickett and D.J. Singh, Phys. Rev. Lett. **72**, 3702 (1994).
[19] H. Michor, T. Holubar, C. Dusek, and G. Hilscher, Phys. Rev. B **52**, 16 165 (1995).
[20] S.A. Carter, B. Batlogg, R.J. Cava, J.J. Krajewski, and W.F. Peck, Jr., Phys. Rev. B **50**, 4216 (1994).
[21] T. Saito, N. Oka, K. Koyama, K. Mizuno, K. Endo, and H. Deguchi, J. Magn. Magn. Mater. **177–181**, 557 (1998); K. Mizuno, T. Saito, H. Fudo, K. Koyama, K. Endo, and H. Deguchi, Physica B **259–261**, 594 (1999).
[22] P. Dervenagas, M. Bullock, J. Zarestky, P. Canfield, B.K. Cho, B. Harmon, A.I. Goldman, and C. Stassis, Phys. Rev. B **52**, 9839 (1995).
[23] F. Gompf, W. Reichardt, H. Schober, B. Renker, and M. Buchgeister, Phys. Rev. B **55**, 9058 (1997).
[24] B.K. Cho, P.C. Canfield, and D.C. Johnston, Phys. Rev. Lett. **77**, 163 (1996).
[25] J. Freudenberger, G. Fuchs, K. Nenkov, A. Handstein, M. Wolf, A. Kreyssig, K.-H. Müller, M. Loewenhaupt, and L. Schulz, J. Magn. Magn. Mater. **187**, 309 (1998).
[26] A. Rustom, A.D. Hillier, and R. Cywinski, J. Magn. Magn. Mater. **177–181**, 1153 (1998).
[27] E. Pellegrin, C.T. Chen, G. Meigs, R.J. Cava, J.J. Krajewski, and W.F. Peck, Phys. Rev. B **51**, 16 159 (1995).
[28] Z. Zeng, D.E. Ellis, D. Guenzburger, and E. Baggio-Saitovitch, Phys. Rev. B **54**, 13 020 (1994).
[29] J.P. Perdew, S. Burke, and M. Ernzerhof, Phys. Rev. Lett. **77**, 3865 (1996).
[30] D. Singh, *Plane Waves, Pseudopotentials and the LAPW Method* (Kluwer Academic, Dordrecht, 1994).
[31] T. Siegrist, R.J. Cava, J.J. Krajewski, and W.F. Peck, Jr., J. Alloys Compd. **216**, 135 (1994).
[32] P. Blaha, K. Schwarz, and J. Luitz, WIEN97 (Vienna University of Technology, Vienna 1997). Improved and updated UNIX version of the original copyrighted WIEN code, which was published by P. Blaha, K. Schwarz, P. Sorantin, and S.B. Trickey, Comput. Phys. Commun. **59**, 399 (1990).
[33] D.D. Koelling and B.N. Harmon, J. Phys. C **10**, 3107 (1977).
[34] J. Sticht and J. Kübler, Solid State Commun. **53**, 529 (1985).
[35] B.C.H. Krutzen and F. Spingelkamp, J. Phys.: Condens. Matter **1**, 8369 (1989).
[36] W.M. Temmerman and P.A. Sterne, J. Phys.: Condens. Matter **2**, 5229 (1990).
[37] D.J. Singh, Phys. Rev. B **44**, 7451 (1991).
[38] P. Wells, P.C. Lanchester, D.W. Jones, and R.G. Jordan, J. Phys. F: Met. Phys. **4**, 1729 (1974).
[39] M. Richter and H. Eschrig, Solid State Commun. **53**, 529 (1985).
[40] M.S.S. Brooks, L. Nordstrom, and B. Johansson, J. Phys.: Condens. Matter **3**, 2357 (1991).
[41] O. Eriksson, R. Ahuja, A. Ormeci, J. Trygg, O. Hjorsstam, P. Soderlind, B. Johansson, and J.M. Wills, Phys. Rev. B **52**, 4420 (1995).
[42] D.M. Bylander and L. Kleinman, Phys. Rev. B **52**, 4420 (1995).
[43] C. Ambosch-Draxl, P. Blaha, and K. Schwarz, J. Phys.: Condens. Matter **6**, 2347 (1994).
[44] M. Richter, J. Phys. D **31**, 1017 (1998).
[45] F.M. Mulder, J.H.V.J. Brabers, R. Coehoorn, R.C. Thiel, K.H.J. Buschow, and F.R. de Boer, J. Alloys Compd. **217**, 118 (1995).
[46] P. Blaha, K. Schwarz, and P. Herzig, Phys. Rev. Lett. **54**, 1192 (1985).
[47] K. Schwarz, C. Ambosch-Draxl, and P. Blaha, Phys. Rev. B **42**, 2051 (1990).
[48] G.H.O. Daalderop, P.J. Kelly, and M.F.H. Schuurmans, Phys. Rev. B **53**, 14 415 (1996).
[49] C.C. Hoellwarth, P. Kalvins, and R.N. Shelton, Phys. Rev. B **53**, 2579 (1996).
[50] H. Schmidt, M. Müller, and H.F. Braun, Physica C **235–240**, 779 (1994).
[51] W.L. McMillan, Phys. Rev. **167**, 331 (1968).
[52] H. Michor, G. Hilscher, R. Krendelsberger, P. Rogl, and F. Bourée, Phys. Rev. B **58**, 15 045 (1998).
[53] G.D. Gaspari and B.L. Gyorffy, Phys. Rev. Lett. **28**, 801 (1972).
[54] W.E. Pickett, Phys. Rev. B **25**, 745 (1982).
[55] The specific heat data presented here are in reasonable agreement with our previous results [$\gamma^{La}=8.4(3)$ mJ/mol K^2, $\gamma^{Lu}=19.5(3)$ mJ/mol K^2 in Ref. 18]; however the accuracy of the measurement and the sample quality has been improved.
[56] M. Divis, H. Michor, S. Khmelevskii, G. Hilscher, P. Blaha, and K. Schwarz Phys. Rev. B (to be published).
[57] R. Coehoorn, K.H.J. Buschow, M.W. Dirken, and R.C. Thiel, Phys. Rev. B **42**, 4645 (1990).
[58] M.E. Hanson, F. Lefloch, W.H. Wong, W.G. Clark, M.D. Lan, C.C. Hoellwarth, P. Klavins, and R.N. Shelton, Phys. Rev. B **51**, 674 (1995).
[59] B.J. Suh, F. Borsa, D.R. Torgeson, B.K. Cho, P.C. Canfield, D.C. Johnston, J.Y. Rhee, and B.N. Harmon, Phys. Rev. B **53**, R6022 (1996).
[60] K. Ikushima, J. Kikuchi, H. Yasuoka, R.J. Cava, H. Takagi, J.J. Krajewski, and W.W. Peck, J. Phys. Soc. Jpn. **63**, 2878 (1994).
[61] D.R. Sanchez, H. Micklitz, M.B. Fontes, and E. Baggio-Saitovitch, J. Phys.: Condens. Matter **9**, 299 (1997).
[62] P. Dufek, P. Blaha, and K. Schwarz, Phys. Rev. Lett. **75**, 3545 (1995).